ELSEVIER

Contents lists available at ScienceDirect

Bioresource Technology

journal homepage: www.elsevier.com/locate/biortech



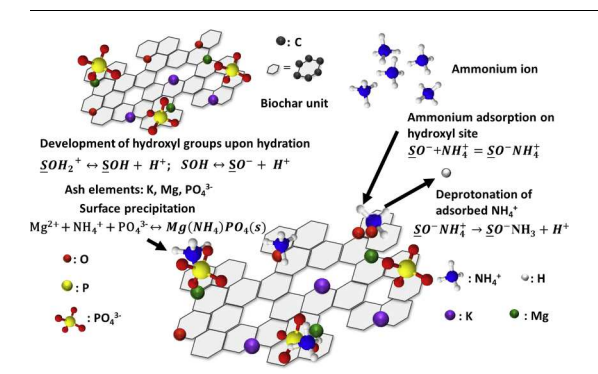
Adsorption characteristics of ammonium ion onto hydrous biochars in dilute aqueous solutions



Ruemei Fan^a, Ching-lung Chen^a, Jui-yen Lin^a, Jing-hua Tzeng^a, Chih-pin Huang^b, Chengdi Dong^c, C.P. Huang^{a,*}

- ^a Department of Civil and Environmental Engineering, University of Delaware, Newark, DE 19716, USA
- ^b Graduate Institute of Environmental Engineering, National Chiao Tung University, Hsin-chu, Taiwan
- ^c Department of Marine Environmental Engineering, National Kaohsiung University of Science and Technology, Kaohsiung, Taiwan

GRAPHICAL ABSTRACT



ARTICLE INFO

Keywords:
Ammonium
Biochar
Heterogeneous adsorption
Surface complexation
Surface precipitation
Slow-release fertilizer

ABSTRACT

This research aims at studying the characteristics of ammonium adsorption onto hydrous bamboo biochar. Results showed that pH played the most important role in ammonium adsorption. High ionic strength enhanced the ammonium adsorption capacity of bamboo biochar. Ammonium adsorption was exothermic and spontaneous. FTIR results showed shift, disappearance, or appearance of specific functional groups on the bamboo biochar surface. Surface precipitation and complex formation contributed to the adsorption of ammonium onto hydrous bamboo biochar. Biochar can be an effective adsorbate for ammonium removal from water. Additionally, the formation of nitrogen containing precipitates on the biochar surface, potentially, leads to the *in-situ* synthesis of slow-release fertilizer.

1. Introduction

The International Biochar Initiative has defined biochar as a solid material obtained from thermochemical conversion of biomass in an oxygen-limited environment. As an old material, biochar has been endowed with ample of new opportunities, e.g., carbon sequestration,

environmental remediation, and energy production (Lehmann, 2009). To date, biochar has received extensive attention mainly because of its potential in agronomic and environmental applications. Pyrolysis of raw biomass is a low-cost operation and can also produces many byproducts, such as valuable biooil and syngas (Ahmad et al., 2014). Biochar can adsorb a wide variety of environmental pollutants because

E-mail address: huang@udel.edu (C.P. Huang).

^{*} Corresponding author.

of its numeral unique physical properties such as highly porous structure and high specific surface area. Additionally, biochar has been increasingly recognized as a highly efficient and cost-effective sorbent because of its abundant multifunctional groups as well as elemental components. Biochar has been used for the removal of specific chemicals such as potassium, nitrogen and phosphorus, which ultimately can be converted to useful fertilizer products (Mohan et al., 2014).

Ammonium is an emerging contaminant. Ammonium volatilization can inhibit the photosynthesis of algae through chlorophyll fluorescence and electron transport. Excessive ammonium in fishing ponds is harmful to the respiratory metabolism of fish, which causes brain swelling via gill injury. Especially, excessive application of fertilizer also increases nitrogen flux to aquatic systems, which may deteriorate surface and ground water quality and bring about eutrophication in water bodies. Therefore, it is therefore of great importance to develop effective technology for the control of ammonium in the aquatic environment.

Efforts toward the control of ammonium flux into the environment have been focused on biological degradation (Reinhart and Basel Al-Yousfi, 1996), advanced oxidation (Murray and Parsons, 2004), and adsorption processes. Among the above methods, adsorption is a relatively simple operation, especially for dealing with solutions of dilute ammonium concentration, and thus has received most attention. Furthermore, among many ammonium adsorbents, there is recent interest on the development of black carbon adsorbent because of its porous structure, large specific surface area, thermostability, which are important properties for ammonium removal from water. Furthermore, the nutrient loaded biochar is an ideal organic fertilizer. A biochar soil management program for the recycling of agricultural wastes and energy production using renewable resources is the most innovative strategy (Lehmann et al., 2006). Currently, biochar also has been applied as a soil amendment to enhance radish yields in the presence of N fertilizer and particularly to produce significant agronomic value in a hard-setting soil (Chan et al., 2007). The great advantage of ammonium-laden biochar is that the post-adsorption product can be reused in the agriculture field as a slowly releasing fertilizer, which has been proved to increases soil fertility and crop productivity (Mohan et al., 2014). Therefore, biochar, in essence, can replace the relatively expensive traditional adsorbents such as activated carbon for ammonium adsorption and become a nitrogen fertilizer that slowly releases nitrogen nutrient to the soil matrix.

There are many studies on the adsorption of ammonium onto biochar (Yao et al., 2012; Hale et al., 2013; Hollister et al., 2013). But there is little agreement on the effect of pertinent parameters on ammonium adsorption capacity. Equally lacking is the mechanistic aspects of ammonium adsorption onto hydrous biochar. (Hale et al., 2013) reported that both unburned cacao shell and corn cob biochar effectively adsorbed ammonium-N (Hale et al., 2013), while (Hollister et al., 2013) found no adsorption of nitrogen onto biochar derived from corn (Zea mays L.) and oak (Quercus spp.). (Yao et al., 2012) reported that nine out of thirteen biochars had little adsorption capacity for nitrogen. The different results reported in the literature can be readily attributed to the use of different types of biochar studied. (Hale et al., 2013) reported that ion exchange was responsible for ammonium adsorption, while (Hollister et al., 2013) reported H-bond formation between ammonium and biochar surface contributed to ammonium adsorption. However, (Yao et al., 2011a) reported that the colloidal and nano-sized MgO particles on the biochar surface were the major binding sites.

The present study is to assess the role of pH, as a maser variable, and other pertinent parameters such as ionic strength and temperature on ammonium adsorption onto hydrous biochar exemplified by bamboo biochar. How to describe the surface acidity of biochar with respect to ammonium adsorption in lieu of its highly heterogeneous and complex nature? What role the ash composition of biochar plays in ammonium adsorption? In order to answer the above equations, this present study aimed at 1) quantifying the surface acidity of biochar, 2) investigating

the effect of parameters, such as pH, particle size, ionic strength, and temperature, on the adsorption of ammonium onto hydrous bamboo biochar, and 3) gaining insight into the adsorption mechanism of ammonium onto hydrous bamboo biochar.

2. Materials and methods

2.1. Chemicals and biochar preparation

Ammonium chloride and sodium chloride were purchased from Fisher Scientific™. Bamboo-derived biochar was purchased from Lewis Chemical Company, Rome, GA, USA and ground into different particle sizes with mortar and pestle in nitrogen-filling chamber. According to the manufacturer, the biochar was prepared by low-temperature pyrolysis at 370 °C of bamboo in the absence of air. The biochar was ground and sieved into different size classes then stored in clean glass bottles with lids until use.

2.2. Ash content and ash element composition

The bamboo biochar samples were dried at 105 °C for two h to obtain the dry weight. The dried bamboo biochar samples were heated at 500 °C in an oven for eight h to obtain the ash content (Song and Guo, 2012). Dried ash was acid digested and the total concentration of elements, namely, K, Ca, Mg, Fe, Mn, and S were determined by using inductively coupled plasma-atomic emission spectroscopy (ICPAES). Total nitrogen (TN) concentration was determined using the Shimadzu 5000A TC/TN analyzer (Song and Guo, 2012).

2.3. Surface characterization of bamboo biochar

The biochar was characterized for specific surface area, surface charge, FTIR, and SEM. The specific surface area was determined by nitrogen gas adsorption at 77 K using a Micromeritics ASAP 2000 automated adsorption apparatus (Norcross, GA) and calculated by the Brunauer–Emmett–Teller (BET) equation. The $\rm N_2$ adsorption isotherm (BET) method determined mesopore-enclosed (< 1.5 nm) surfaces. Prior to nitrogen gas adsorption, samples were degassed at 300 °C in a vacuum to 10^{-3} Torr (Song and Guo, 2012).

The zeta potential of bamboo biochar was measured in three levels of ionic strength at $1\times 10^{-3},~1\times 10^{-2},~\text{and}~1\times 10^{-1}\,\text{M}$ NaCl, individually, using Malvern Nano Zeta Sizer (Chiang et al, 2002). The zeta potential measurements were carried out immediately after pH adjustment.

Scanning electron microscopy (SEM, JEOL JSM-6400) coupled with dispersive X-ray spectroscopy (EDS, Oxford Instruments Link ISIS) was used to compare the structure and surface characteristics of biochar before and after ammonium adsorption. Surface element analysis was also conducted simultaneously with the SEM at the same surface locations using energy dispersive X-ray spectroscopy. The EDS can provide rapid qualitative, or with adequate standards, semi-quantitative analysis of elemental composition with a sampling depth of $1{\text -}2\,\mu\text{m}$. The characteristics of the ammonium-loaded biochar were compared with the raw biochar to reveal the mode of ammonium adsorption.

Fourier Transform Infrared (FTIR) spectral analysis of the biochar was carried out to characterize the surface organic functional groups before and after ammonium adsorption using a Bruker Vertex 70 spectrometer (Bruker Optics, Billerica, MA) fitted with a Pike Technologies Miracle attenuated total reflectance (ATR) accessory (Madison, WI) with a diamond crystal plate. The spectra were obtained at 8 cm $^{-1}$ resolution from 650 to 4000 cm $^{-1}$ with 128 scans.

2.4. Batch ammonium adsorption

Biochar $(0.1\ g)$ with a uniform particle size of 88 μm was added to a 250 mL plastic bottle containing 100 mL solution of ammonium salts at

different concentrations. Sodium chloride (0.01 M), was added as ionic strength to simulate industrial wastewater. HCl (0.1–1 M) and NaOH (0.1–1 M) were used to adjust the pH during the adsorption experiment.

To study the effect of particle size on ammonium adsorption, 0.25 g Biochar with the different particle size of 88, 193, and 917 μm , individually, was added to 250-mL plastic bottles each containing 100 mL of 40 mM ammonium chloride solution prepared with deionized water. Then sodium chloride was added at 0.01 M as ionic strength and the other experimental steps followed were described above. To study the effect of ionic strength on ammonium adsorption, samples were prepared in the presence of NaCl at $1\times 10^{-2},\ 5\times 10^{-2}$ and $1.0\times 10^{-1}\, M$. To study the effect of temperature, samples were prepared as above except that the temperature was held constant at 277, 285, 293, 301, and 309 K, individually, with a temperature controller.

After sample preparations, the suspensions were mixed over a shaker (manufactured by Lab-Line Instruments Company) at 150 S per min at different time (for kinetics study) and 24 h (for equilibrium study). The suspensions were then filtered through 0.45- μ m membranes to collect the filtrate for the analysis of residual ammonium concentration using ion chromatography (Dionex ICS-1100).

3. Results and discussion

3.1. Ash content and element composition

Table 1 shows that the ash content of the bamboo biochar was 5.80 and 5.22% on a wet and dry basis, respectively. The difference was attributed to its moisture content of 9.95%. The bamboo biochar used in this study had a relatively higher ash content than samples reported by Liu et al. (2014). As indicated above, a higher ash content of the bamboo biochar may be derived from its low pyrolysis temperature of about $370\,^{\circ}\text{C}$.

To some extent, the ash content can be determined for the mineral-rich bamboo biochar. The inorganic elements comprising of minerals at the biochar surface can be separated from the carbonaceous matrix. It was reported that the increase in inorganic constituents in ash can affect the pH of the solution containing the biochar (Galanakis, 2017). Table 1 shows the element composition of the ash, e.g., Al, As, Ca, Cd, Cr, Cu, Fe, K, Mg, Mn, Na, Ni, Pb, P, S, and Zn, in the bamboo-derived biochar.

Generally, the mineral content of K, Al, Ca and Mg was high in the ash, especially K, which content was 40.0 g-kg⁻¹. K was the most

Table 1
Physic-chemical properties of bamboo biochar.

BET surface area (m ² /g)	229.46 (88 μm)	
Ash content (%)	Moisture	10.0
	Solid	90.0
	wet weight basis	5.22
	dry weight basis	5.8
Elemental composition (mg/kg)	Al	847.21
	As	< det
	Ca	2968.47
	Cd	< det
	Cr	9.22
	Cu	42.75
	Fe	2188.96
	K	40040.41
	Mg	1573.12
	Mn	373.58
	Na	98.80
	Ni	3.63
	Pb	15.22
	P	4239.83
	S	581.47
	Zn	126.64

abundant inorganic fraction of ash content in addition to other minerals including Ca and Mg. Note that these minerals are present in oxide forms, as such the solution containing the biochar tended to exhibit alkaline pH value. The results were consistent with that of other biochar samples prepared from corncobs by fast pyrolysis (Mullen et al., 2010). The high inorganic constituent of K, Al, Ca, and Mg are postulated to promote the formation of O-containing functional groups, such as hydroxyl and carboxyl groups on the biochar surface (Bourke et al., 2007). Notably, both Fe and Mn contents were found at a high concentration of 2188.9 and 373.7 mg-kg⁻¹, respectively.

3.2. Specific surface area

The specific surface area of the raw bamboo biochar was $24.3~\text{m}^2\text{g}^{-1}$ without acid treatment, which was much higher than most of those previously reported in the literature: in the range from 0.70 to $81.1~\text{m}^2\text{g}^{-1}$ (Chen et al., 2011; Li et al., 2017; Spokas et al., 2012; Yao et al., 2012). Results in Table 1 shows that acid treatment significantly increases the specific surface area of biochar. Note that the specific surface area was $229.4~\text{m}^2\text{-g}^{-1}$ after treatment with 0.1 M acid for 1 h, which was 9.42 times that of biochar without acid treatment.

3.3. Surface charge

The surface acidity of hydrous biochar is derived from hydroxyl, carboxyl, and phenolic functional groups (Jia et al., 2013). Recent studies have shown that many biochars derived from various feedstocks exhibit negative charge and high mineral content, such as alkali (e.g., K) and alkali earth (e.g., Ca, Mg), which contribute to high alkalinity of the solution (Bourke et al., 2007; Mukherjee et al., 2011; Yuan et al., 2011). Results in Fig. 1 show that higher ionic strength, e.g., $1\times 10^{-1}\,\mathrm{M}$ NaCl, can reduce the zeta potential of the bamboo biochar compared to that of relatively lower ionic strength, e.g., $1\times 10^{-2}\,\mathrm{M}$ or $1\times 10^{-3}\,\mathrm{M}$ NaCl.

When an H-carbon is placed in water, positive charge evolves. Likewise, when a L-carbon is introduced into water, a negative charge will be observed (Chiang et al., 2002). Exposing an H-carbon to atmospheric oxygen gradually converts it to L-carbon.

The zeta potential of the bamboo biochar changed as a function of pH. At a specific pH, the zeta potential, and thus surface charge, is zero, which is the pH at zero-point of charge (pH_{zpc}). In this study, the pH_{zpc}

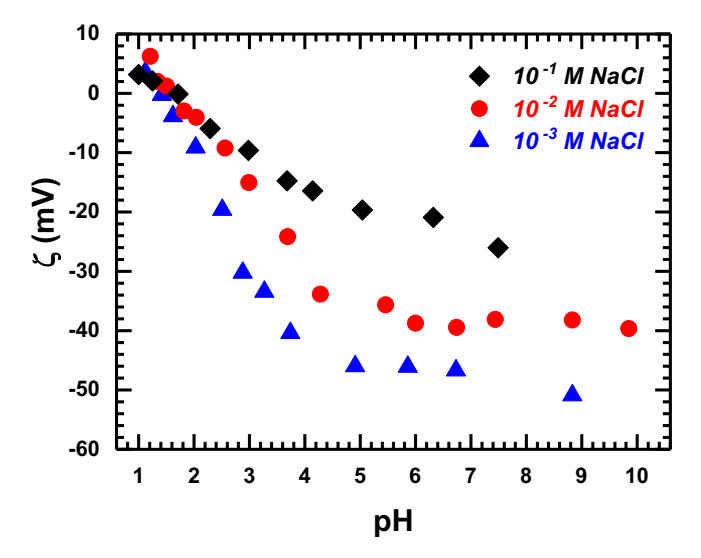


Fig. 1. Zeta potential (ζ) of bamboo biochar as a function of pH under different ionic strength. Experimental conditions: [Biochar] = 2.5 g/L, equilibrium time = 12 h, T = 20 °C, [particle size] = 88 μ m.

of the bamboo biochar was close to 1.5 ± 0.2 . Obviously, the surface charge characteristics of the bamboo biochar were influenced by pH, which implied that OH^- and H^+ ions potentially are the major potential determining ions. Result also indicated that NaCl ions were not specifically absorbed onto the bamboo biochar. Similar results have been reported by (Yuan et al., 2011) who determined the zeta potential as a function of pH in solution containing biochar prepared from crop residue.

3.4. Surface acidity

Upon hydration, hydroxyl groups developed on the hydrous carbon surface. The hydroxyl groups behave as weak BrÖnsted acids-bases according to the following protonation/deprotonation equilibria:

$$SOH_2^+ \leftrightarrow SOH + H^+; K_{a1}^{int}$$
(1)

$$SOH \leftrightarrow SO^{-} + H^{+}; K_{a2}^{int}$$
 (2)

where SOH_2^+ , SOH, and SO^- are the protonated, neutral, and ionized surface hydroxyl groups, respectively. The intrinsic acidity constants, K_{a1}^{int} and K_{a2}^{int} are defined according to the law of mass action, Eqs. (3) and (4), respectively:

$$K_{a1}^{int} = \frac{\{SOH\}\{H^{+}\}}{\{SOH_{2}^{+}\}}$$
(3)

$$K_{a2}^{int} = \frac{\{SO^{-}\}\{H^{+}\}}{\{SOH\}}$$
(4)

where $\{i\}$ stands for the surface concentration (or activity) of the ith species. From the above equations, the zero-point charge of pH, i.e., pH_{zpc} , is the average value of pK_{a1}^{int} and pK_{a2}^{int} , i.e.,

$$pH_{zpc} = \frac{1}{2}(pK_{a1}^{int} + pK_{a2}^{int})$$
 (5)

The total number of surface BrÖnsted acidity sites, N_T , is therefore the sum of the three hydroxyl species, i.e.,

$$N_T = \{SOH_2^+\} + \{SOH\} + \{SO^-\}$$
(6)

At pH < pH_{zpc} , { SOH_2^+ } and {SOH} are the predominant surface hydroxyl species, i.e.,

$$N_T = \{SOH_2^+\} + \{SOH\}$$
(7)

And at pH $> pH_{zpc}$, {SO⁻} and {SOH} groups are the predominant surface hydroxyl species, i.e.,

$$N_T = \{SO^-\} + \{SOH\}$$
- (8)

Furthermore, at pH $< pH_{zpc}$,

$${SOH_2^+} = \frac{S_A}{F} \sigma^+$$
 (9)

and at pH > pH_{zpc}

$$\{SO^-\} = \frac{S_A}{F} \sigma^- \tag{10}$$

where S_A is the total surface area present in the solution (m²-L⁻¹), and F is the Faraday constant (96498 C-mol⁻¹). [SO⁻} is the negatively charged surface hydroxyl group (M) and σ^- is the negative surface charge density (C-m⁻²). By combining the above equations, i.e., Eqs.

Table 2BrÖnsted acidity of hydrous bamboo biochar in NaCl electrolyte.

NaCl (M)	N _T (mol/m ²)	pK_{a1}^{int}	pK_{a2}^{int}	$\mathrm{pH}_{\mathrm{zpc}}$
1×10^{-3}	5.58×10^{-5}	0.36	2.64	1.50
1×10^{-2}	1.24×10^{-5}	0.23	2.77	1.50
1×10^{-1}	1.37×10^{-5}	0.18	2.82	1.50

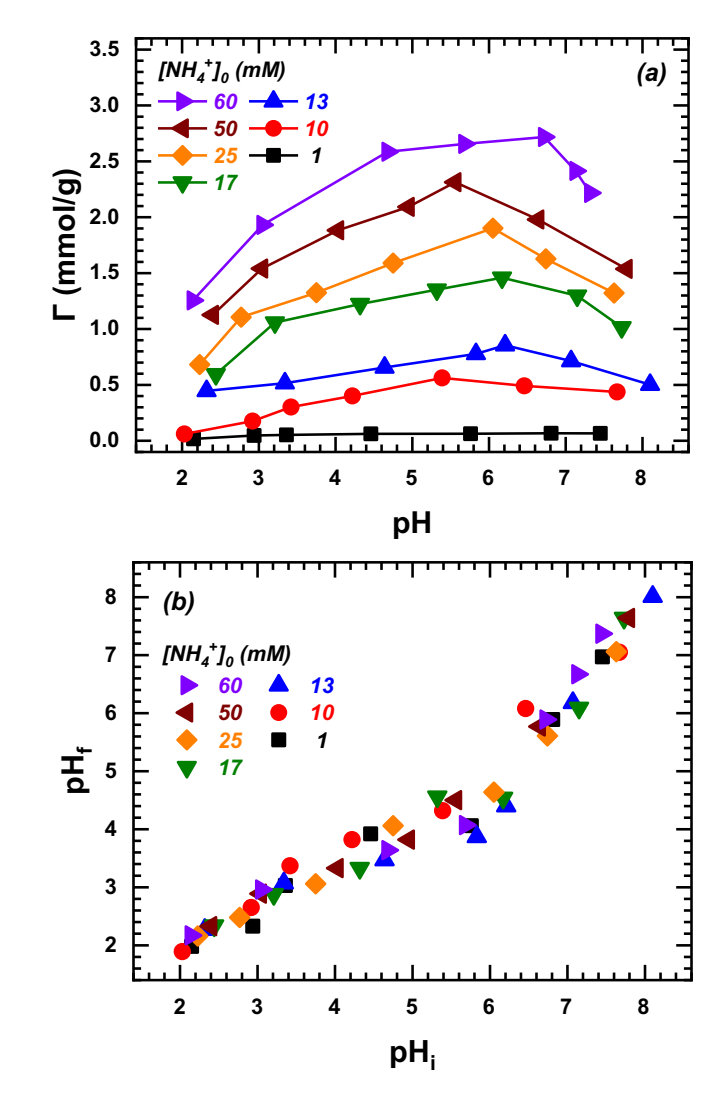


Fig. 2. Adsorption of ammonium onto hydrous bamboo biochar. (a) Adsorption capacity as a function of pH; (b) change of pH upon ammonium adsorption. Experimental conditions: [Biochar] = 1 g/L, equilibrium time = 12 h, $T = 20 \,^{\circ}\text{C}$, [particle size] = $88 \, \mu \text{m}$, [NaCl] = $10 \, \text{mM}$.

(1)–(4), and after further mathematical arrangement, one has: at pH < pH_{zpc} ,

$$\frac{1}{\{H^{+}\}} = \frac{N_{T}}{K_{a1}^{int}} \left(\frac{1}{\sigma^{+}}\right) - \frac{1}{K_{a1}^{int}}$$
(11)

and at pH $> pH_{zpc}$,

$$\{H^{+}\} = N_{T} K_{a2}^{int} \left(\frac{1}{\sigma^{-}}\right) - K_{a2}^{int}$$
 (12)

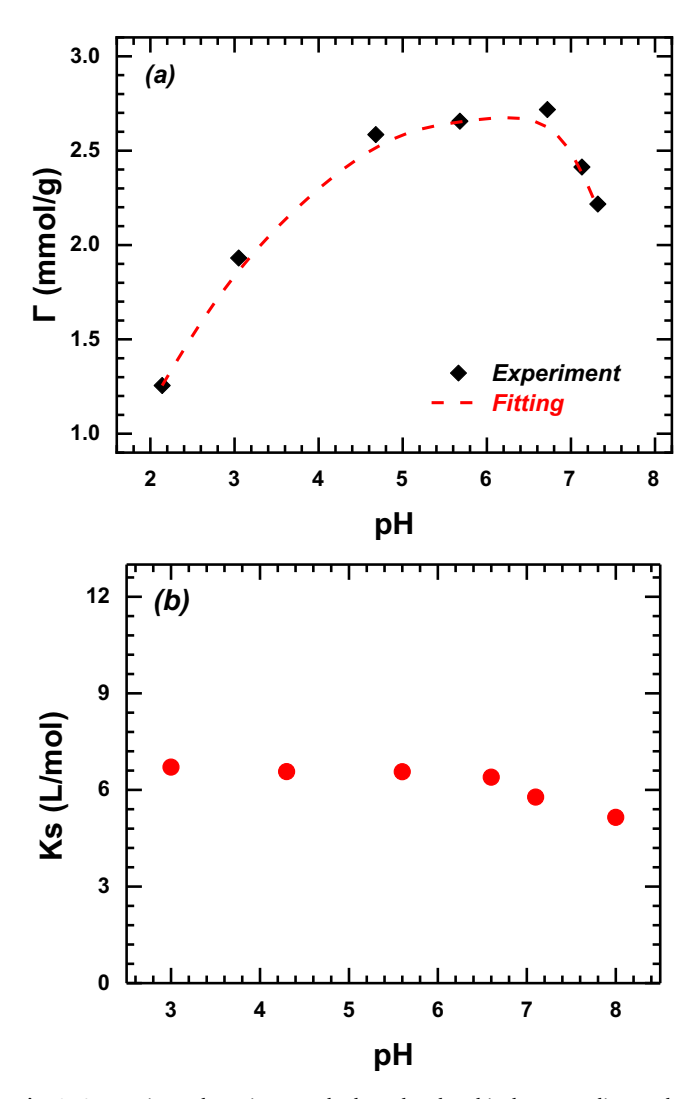


Fig. 3. Ammonium adsorption onto hydrous bamboo biochar according to the surface complex formation model: $SO^- + NH_4^+ \leftrightarrow SO^+NH_4^+$; K_s ; (a) fitted adsorption isotherm as a function of pH; (b) stability constant of surface complexes as a function of pH. Experimental conditions: $[NH_4^{\ +}]_0 = 60 \, \text{mM}$, $[NaCl] = 10 \, \text{mM}$, $[Biochar] = 1 \, \text{g/L}$, equilibrium time = 12 h, $T = 20 \, ^{\circ}\text{C}$.; $[particle \ size] = 88 \, \mu m$, $S_T = 5 \times 10^{-5} \ \text{mol/m}^2$; $[specific \ surface \ area] = 229 \, \text{m}^2/\text{g}$. average $[Ks] = 5.4 \, \text{M}^{-1}$.

A plot of $\frac{1}{\{H^+\}}$ versus $\frac{1}{\sigma^+}$, (or $1/\{H^+\}$ versus $\{\underline{SO}^-\}$) for the positive surface and of $\{H^+\}$ versus $\frac{1}{\sigma^-}$ (or $\{H^+\}\{SO^-\}$ versus $\{SO^-\}$) for the negative surface will yield intercepts and slopes from which the intrinsic acidity constants K_{a1}^{int} and K_{a2}^{int} , and the total number of surface sites, N_T , can be calculated. The surface acidity enables the calculation of surface speciation.

Table 2 shows the surface acidity of the bamboo biochar. The pK_{a1}^{int} and pK_{a2}^{int} of the bamboo biochar was relatively smaller than other types of carbon (Corapcioglu and Huang, 1987), which indicated that the bamboo biochar had the strong BrÖnsted acid characteristics. Fig. 2 shows the distribution of surface hydroxyl species as a function of pH. Results showed that $[SO^-]$ was the dominant species over the pH range studied.

3.5. Effect of pH, ionic strength, and temperature

Fig. 2a shows the effect of pH on ammonium adsorption. Results show that pH plays an important role on ammonium adsorption onto

hydrous biochar. As shown in Fig. 2a, the optimal pH of ammonium adsorption was around 6.5. The ammonium absorption capacity continuously increased until pH was between 6 and 7, and then decreased. It is obvious that pH is a master variable on ammonium adsorption because both the surface speciation of biochar and ammonium speciation are functions of pH. Accordingly, there is formation of surface complexes between NH_4^+ and the negatively charged surface hydroxyl species, SO^- :

$$SO^- + NH_4^+ = SO^- NH_4^+; K_s$$
 (13)

The stability constant, K_s , can be calculated accordingly based on the surface acidity and the stoichiometry of the surface complex formation. At 20 °C and 10^{-2} M NaCl, K_s was $5.4\,M^{-1}$. Fig. 3a shows the fitted adsorption capacity as a function of pH based on the surface complex formation mechanism, i.e., Eq. (13). Fig. 3b shows that the stability constant of the surface complexes remains relatively constant with respect to pH and that the energy of adoption is relatively small. (Hou et al., 2016) have reported similar pH effect on ammonium adsorption onto biochar prepared from giant reed.

It is interesting to note that the pH values drop in the pH range of 4.0 to 7.0 (Fig. 2b). Obviously, there is deprotonation of the surface $\mathrm{NH_4}^+$ complexes, which results in the formation of poorly adsorbed $\mathrm{NH_3}$ as evident of the relatively small stability constant, $\mathrm{K_s} = 5.4$ (Fig. 3b), i.e.,

$$SONH_4^+ \rightarrow SONH_3^- + H^+ \tag{14}$$

As will be discussed later, due to the presence of ash elements, specifically, ${\rm Mg^{2}}^+$ and ${\rm PO_4}^{3-}$, it is likely that surface precipitation in the form of ${\rm MgNH_4PO_4}$ (struvite) might take pace and play a role on ammonium adsorption. Although struvite can form over a wide pH range, extreme acid or alkaline condition are unfavorable for struvite precipitation (Fujimoto et al., 1991). In summary, surface complex formation and surface precipitation are responsible for the removal of ammonium ion from dilute aqueous solution in the presence of bamboo biochar.

Several authors have reported the effect of ionic strength on the adsorption capacity of absorbents (Al-Degs et al., 2008; Liu et al., 2011; Sepulveda and Santana, 2013). As shown in Fig. 4, the adsorption capacity of ammonium unto the hydrous bamboo biochar increased with an increase in ionic strength. In principle, if there is competition

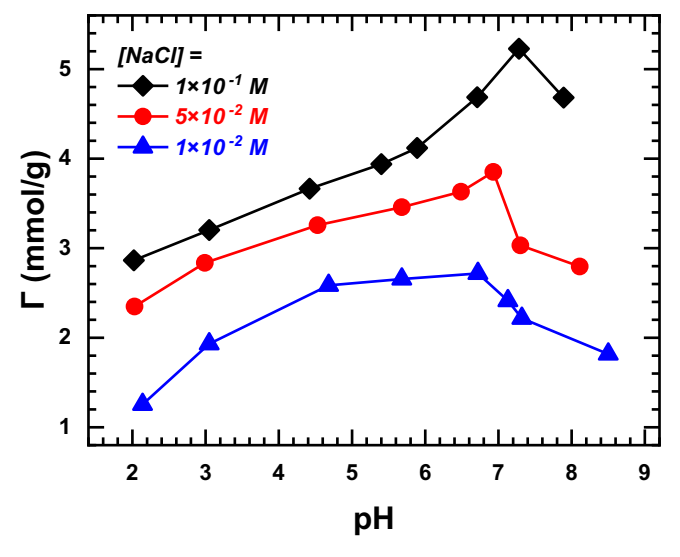


Fig. 4. Ammonium adsorption onto hydrous bamboo biochar as affected by ionic strength. Experimental conditions: $[NH_4^+]_0 = 40 \text{ mM}$, [biochar] = 1 g/L, [NaCl] = 10 mM, equilibrium time = 12 h, T = 20 °C, $[particle \text{ size}] = 88 \mu\text{m}$.

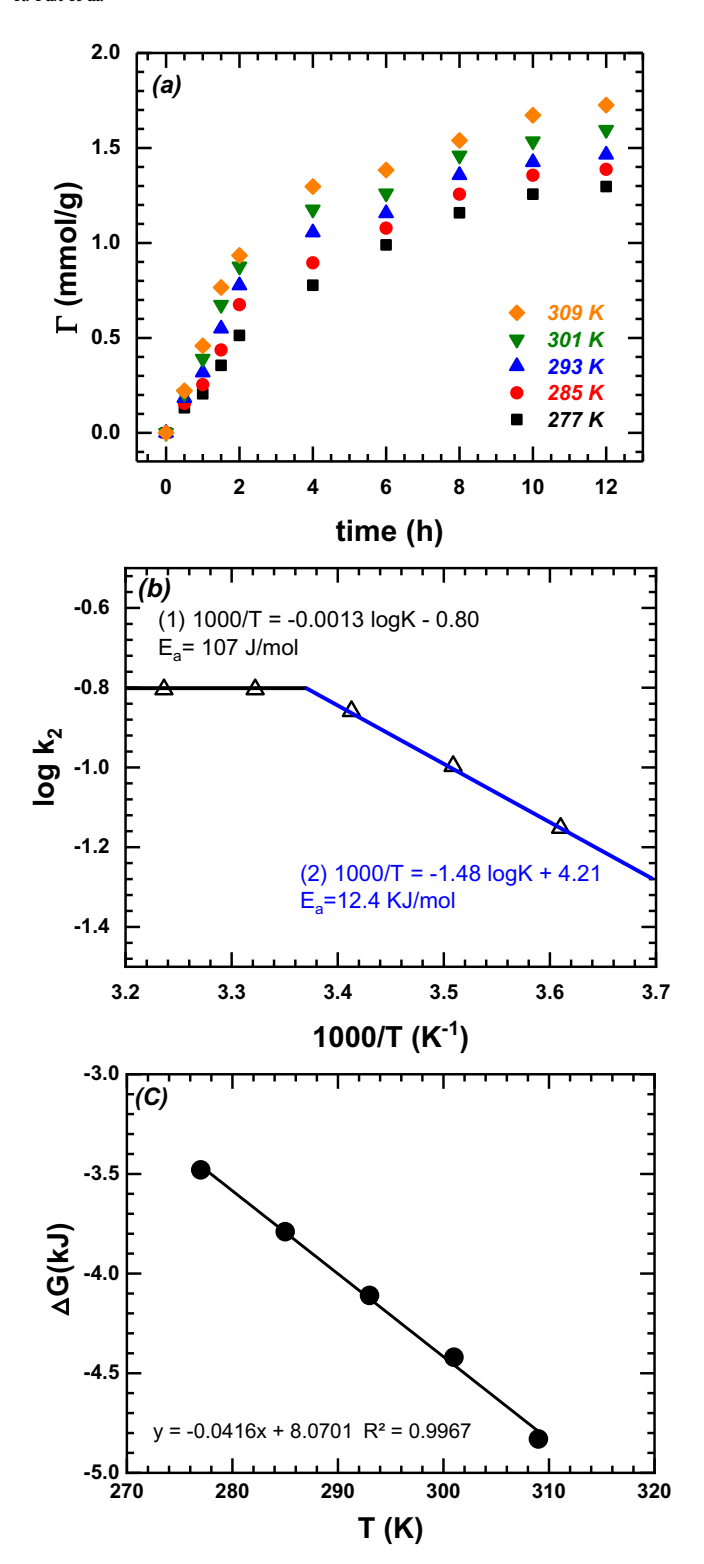


Fig. 5. Ammonium adsorption onto hydrous bamboo biochar as affected by temperature. (a) Adsorption capacity as a function of time; (b) linearized Arrhenius plot; (c) Plot of Gibbs free energy as a function of temperature. Experimental conditions: $[\mathrm{NH_4}^+]_0 = 40\,\mathrm{mM}$, $[\mathrm{biochar}] = 1\,\mathrm{g/L}$, equilibrium time = 12 h, T = 20 °C, $[\mathrm{particle\ size}] = 88\,\mu\mathrm{m}$, $[\mathrm{NaCl}] = 10\,\mathrm{mM}$.

between $\mathrm{NH_4}^+$ and cations such as Na^+ for surface sites, $\mathrm{NH_4}^+$ adsorption will decrease with increase in ionic strength. However results of zeta potential measurements show that Na^+ adsorption decreases with increase in NaCl concentration, which should favor ammonium ion adsorption due to decrease in Na^+ ion competition for surface sites.

The results show significant increase in ammonium ion adsorption with increases in ionic strength. It is postulated that van der Waals, ion–dipole and dipole–dipole interactions result in the formation of aggregates that incorporate ammonium ions and other inorganic ions such as ${\rm Mg}^{2+}$ and ${\rm PO_4}^{3-}$ on the biochar surface. Accordingly, high salt concentration results in high ammonium adsorption capacity. The results were consistent with that reported by other studies that ion adsorption increase with an increase in ionic strength (Al-Degs et al., 2008; Alberghina et al., 2000; Germán-Heins and Flury, 2000; Newcombe and Drikas, 1997; Sepulveda and Santana, 2013).

Fig. 5a shows the adsorption of ammonium onto hydrous bamboo biochar at 277, 285, 293, 301, and 309 K, respectively, as a function of time. The data were fitted by the pseudo-second order kinetics equation. (Note that separate analysis of the adsorption data as a function of time reveals that the pseudo-second order equation fits better the data than the pseudo-first order equation.)

The rate constant, \mathbf{k}_2 , is related to the activation energy by the Arrhenius equation:

$$k_2 = A \exp(-E_a/RT) \tag{15}$$

Fig. 5b shows the linear Arrhenius plot, i.e., $\log k_2$ versus 1/T, from which two kinetics regimes and corresponding activation energy E_a were observed, i.e., $E_a = 0.11$ and $12.4 \, \text{kJ-mol}^{-1}$, at T > 298 and $T < 298 \, \text{K}$, respectively. The results clearly indicated that, ammonium adsorption was surface reaction controlled and mass transfer controlled at $T < 298 \, \text{K}$ and $T > 298 \, \text{K}$, respectively.

Furthermore, data in Fig. 5a can be used to calculate the equilibrium adsorption constant, K_s , according to Eq. (13). With K_s values known, the Gibbs free energy of adsorption (ΔG°) can be calculated:

$$\Delta G^0 = -RT ln K_s \tag{16}$$

From the Gibbs equation, the enthalpy, ΔH^o , and entropy, Δs° , of adsorption were calculated according to Eq. (16) by plotting ΔG° versus T (Table 3):

$$\Delta G^{\circ} = \Delta H^{\circ} - T \Delta S^{\circ} \tag{17}$$

The ΔG^o values were in the range of -3.48 to -4.83 kJ mol $^{-1}$. The ΔH^o and ΔS^o value were -8.07 kJ mol $^{-1}$ and 41.6 J mol $^{-1}$ K $^{-1}$, respectively (Table 3). It has been suggested that the process will be physical adsorption controlled at bonding strength smaller than 84 kJ-mol $^{-1}$, otherwise, chemical controlled adsorption if the bonding strength is within $84 \sim 420$ kJ-mol $^{-1}$ as in the case of gaseous adsorption (Faust and Aly, 1987). However, it has been reported that adsorption from aqueous solution onto hydrous biochar follows a different adsorption mechanism; a combination of both physical and chemical adsorption processes (Mattson and Mark, 1971).

Higher temperature appears to favor adsorption slightly. Result showed that ammonium adsorption is an exothermic reaction. The result was consistent with previous reports that heavy metal uptake by biochar increased with increase in temperature (Chen et al., 2011; Liu and Zhang, 2009; Mohan et al., 2007). Increase in temperatures provides sufficient energy enabling ammonium ion transport into the interior pore structure of the biochar. Furthermore, higher temperature facilitates creation of new active sites and the penetration by adsorbed

 Table 3

 Thermodynamic parameters of ammonium adsorption.

Temperature (K)	K (1/M)	ΔG_0 (KJ/mol)	ΔH_0 (KJ/mol)	ΔS ₀ (J/mol K)
277	4.53	-3.48	-8.07	41.6
285	4.96	-3.79	_	_
293	5.40	-4.11	_	_
301	5.86	-4.42	_	_
309	6.56	-4.83	_	_

Experimental conditions: [ammonia] = 40 mM; [biochar] = 1 g/L; [NaCl] = 10^{-2} M, $S_T = 8.72 \times 10^{-3}$ M, pH = 7.0.

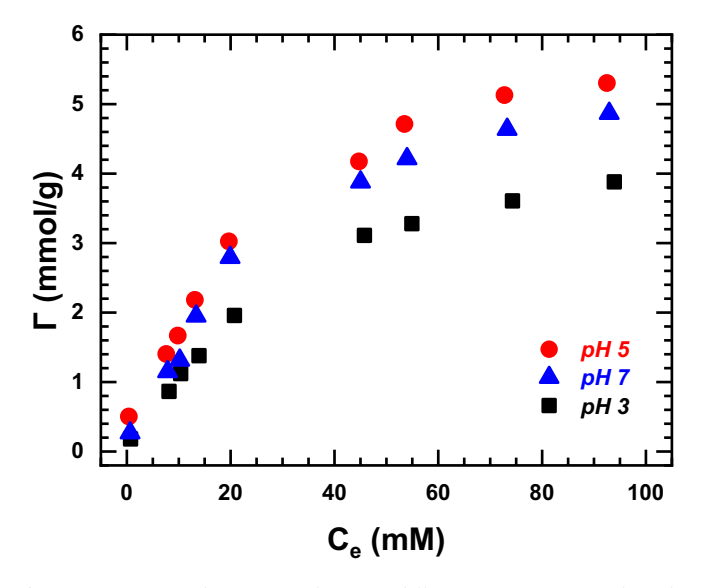


Fig. 6. Ammonium adsorption isotherms at different pH. Experimental conditions: [biochar] = 1 g/L, equilibrium time = 12 h, $T = 20\,^{\circ}C$, [particle size] = $88\,\mu m$, [NaCl] = $10\,m M$.

ions into micropores (Al-Degs et al., 2008).

The results were in agreement with others that adsorption process was exothermic due to heat release after bond formation between solute and adsorbate (Ruthven, 1984). Nonetheless, other authors have reported endothermic adsorption of pollutants dependent on different types of adsorbents (Guo et al., 2005; Namasivayam and Kavitha, 2002; Netpradit et al., 2004). The results on temperature effect were in agreement with several current studies (Liu et al., 2011; Liu and Zhang, 2009; Sepulveda and Santana, 2013). Finally, it is noted that the adsorption of ammonium onto hydrous bamboo biochar was a spontaneous process as indicated from the negative free energy.

3.6. Mode of ammonium adsorption

According to the Giles and Smith classification, L₂-behavior adsorptive process was established on the premise of monolayer adsorption, with the formation of no more than one layer of adsorption (Giles and Smith, 1974). L₂-type isotherms generally indicate that ionic solute adsorption was weaker than solvent molecules.

Ammonium adsorption density as a function of equilibrium ammonium concentration in Fig. 6 were analyzed by the (Langmuir, 1918) and the (Freundlich, 1906) adsorption isotherms, respectively. The correction constants, r^2 , of the Langmuir model was 0.9659, 0.9545, and 0.9573, respectively, which were slightly less than that of the Freundlich model, 0.9907, 0.9763, and 0.9832, respectively. Therefore, the Freundlich adsorption isotherm appeared to be more favorable in describing the adsorption of ammonium onto the hydrous bamboo biochar surface than the Langmuir model. In light of the heterogeneity nature of the biochar surface, ammonium adsorption Å² would be complex that multiple layer adsorption onto sites of non-uniform energy distribution could occur. Based on the Langmuir adsorption isotherm, the maximum adsorption capacity was estimated to be 5.29, 6.49, and 6.38 mM-g⁻¹ at pH 3, 5, and 7 respectively. The parking space per ammonium ion was 0.76, 0.62, and 0.63, per molecule, respectively. The average ionic radius of ammonium is 1.52 Å² (Sidey, 2016), which is equivalent to 7.3 Å² per molecule. Results clearly show the possibility of multi-layer adsorption, e.g., ca. 10-12 layers.

Results on the FTIR spectra of biochar before and after ammonium adsorption show that upon ammonium adsorption, there are changes in peak height of aromatic carboxyl/carbonyl C=O stretch $(1670 \sim 1820~\text{cm}^{-1})$, amine bending N-H ($\sim 1600~\text{cm}^{-1}$), aromatic C=C stretch $(1400 \sim 1600~\text{cm}^{-1})$, alcohol C-O $(1050 \sim 1150~\text{cm}^{-1})$,

and amine stretch C-N (1080~1360 cm⁻¹). All of the above chemical bands obviously changed with pH compared to that of raw biochar. The aromatic C=O peak position of biochar happened to red shift after adsorbing ammonium ion. The band intensities of C=O dramatically decreased after adsorption of ammonium on the biochar surface. The C=C bands on the bamboo biochar surface almost vanished after adsorbing ammonium ions. The other polar alcohol (C=O) group exhibited a lower peak magnitude after adsorption of ammonium upon the bamboo biochar. The above spectra changes could be attributed to ammonium adsorption, indicating that there was interaction between ammonium and biochar surface function groups (Kizito et al., 2015).

Results on the SEM imaging of the before and after ammonium adsorption on biochar show a wide spread of nano-scale crystals on the carbon surface. The EDS spectra identify a Mg peak, indicating another potential dominant adsorption site, which was consistent with (Yao et al., 2011b) who studied phosphate adsorption on biochar prepared from anaerobically digested sugar beet tailings. The nano-scaled metal oxide particles may be involved with the adsorption of ammonium. Meanwhile, a P-phosphorus peak was also detected on the bamboo biochar surface. Based on the above observation, the following reaction contributing to ammonium adsorption onto the bamboo biochar surface can be suggested:

$$Mg^{2+} + NH_4^+ + PO_4^{3-} \to MgNH_4PO_4(s)$$
 (18)

Surface precipitation taking place between ammonium and surface magnesium and phosphate, $MgNH_4(PO_4)(s)$ (pK_{sp} = 12.56) (Bhuiyan et al., 2007), which resulted in the formation of less insoluble struvite. Even though the solubility product of $Mg_3(PO_4)_{2,}$ pK_{sp} = 23.98, is less than that of struvite, it is easier to form struvite precipitate since the concentration of ammonium is higher than that of phosphate in the solution phase. (Flores-Cano et al., 2013) also reported cadmium substituting for calcium as a major adsorption mechanism of ammonium on the calcareous surface layer of eggshell. Elemental nitrogen was present on the bamboo biochar surface after ammonium adsorption while there was no elemental nitrogen on the biochar surface before ammonium adsorption. Due to the limitation of SEM-EDS detection, it is difficult to identify whether light elements such as nitrogen can be adsorbed on the biochar surface by using the SEM-EDS method except at condition where nitrogen adsorption density was high. However, in our study, nitrogen was indeed found on the bamboo biochar surface.

Based on FTIR, SEM-EDS, and zeta potential measurements, it is plausible to visualize the adsorption of ammonium ion on the bamboo biochar surface as result of the following pathways: (1) surface complexation between ammonium and surface hydroxol species contributed from the hydration of surface carbon and nanoscaled metal oxides, (Eq. (13)) (2) surface co-precipitation as Mg(NH₄)PO₄(s), and (3) the formation of NH₄-C(π) bonding between ammonium and delocalized lone-pair π electrons in bamboo biochar.

4. Conclusion

Ammonium ions can be effectively absorbed on the bamboo biochar surface at the maximum adsorptive capacity of $6.38\,\mathrm{mM}\text{-g}^{-1}$. Solution pH plays a major role on ammonium adsorption. Particle size of biochar in the range of $88\text{-}917\,\mu\text{m}$, did not have significant influence on ammonium adsorption. Interestingly, higher ionic strength enhanced the adsorption of ammonium, which indicated the possible contribution of physical reaction, i.e., electrostatic force, specific chemical bonds, and surface precipitation to ammonium adsorption. Adsorption process was endothermic and spontaneous.

Acknowledgements

This work was provided by US NSF IOA grand number 1632899 to CPH.

Appendix A. Supplementary data

Supplementary data to this article can be found online at https://doi.org/10.1016/j.biortech.2018.10.064.

References

- Ahmad, M., Rajapaksha, A.U., Lim, J.E., Zhang, M., Bolan, N., Mohan, D., Vithanage, M., Lee, S.S., Ok, Y.S., 2014. Biochar as a sorbent for contaminant management in soil and water: a review. Chemosphere 99, 19–33.
- Al-Degs, Y.S., El-Barghouthi, M.I., El-Sheikh, A.H., Walker, G.M., 2008. Effect of solution pH, ionic strength, and temperature on adsorption behavior of reactive dyes on activated carbon. Dyes Pigm. 77 (1), 16–23.
- Alberghina, G., Bianchini, R., Fichera, M., Fisichella, S., 2000. Dimerization of Cibacron Blue F3GA and other dyes: influence of salts and temperature. Dyes Pigm. 46 (3), 129–137.
- Bhuiyan, M.I.H., Mavinic, D.S., Beckie, R.D., 2007. A solubility and thermodynamic study of struvite. Environ. Technol. 28 (9), 1015–1026.
- Bourke, J., Manley-Harris, M., Fushimi, C., Dowaki, K., Nunoura, T., Antal, M.J., 2007. Do all carbonized charcoals have the same chemical structure? 2. A model of the chemical structure of carbonized charcoal. Ind. Eng. Chem. Res. 46 (18), 5954–5967.
- Chan, K.Y., Van Zwieten, L., Meszaros, I., Downie, A., Joseph, S., 2007. Agronomic values of greenwaste biochar as a soil amendment. Soil Res. 45 (8), 629–634.
- Chen, X., Chen, G., Chen, L., Chen, Y., Lehmann, J., McBride, M.B., Hay, A.G., 2011. Adsorption of copper and zinc by biochars produced from pyrolysis of hardwood and corn straw in aqueous solution. Bioresour. Technol. 102 (19), 8877–8884.
- Chiang, H.-L., Huang, C.P., Chiang, P.C., 2002. The surface characteristics of activated carbon as affected by ozone and alkaline treatment. Chemosphere 47 (3), 257–265.
- Corapcioglu, M.O., Huang, C.P., 1987. The adsorption of heavy metals onto hydrous activated carbon. Water Res. 21 (9), 1031–1044.
- Faust, S.D., Aly, O.M., 1987. Adsorpion Processes for Water Treatment. Guiford Butterworth Scientific Ltd. Publishers, pp. 522.
- Flores-Cano, J.V., Leyva-Ramos, R., Mendoza-Barron, J., Guerrero-Coronado, R.M., Aragón-Piña, A., Labrada-Delgado, G.J., 2013. Sorption mechanism of Cd(II) from water solution onto chicken eggshell. Appl. Surf. Sci. 276, 682–690.
- Freundlich, H., 1906. Adsorption in Solution. Z. Phys. Chem. 57 (384-470).
- Fujimoto, N., Mizuochi, T., Togami, Y., 1991. Phosphorus fixation in the sludge treatment system of a biological phosphorus removal process. Water Sci. Technol. 23 (4–6), 635–640.
- Galanakis, C.M., 2017. Handbook of Coffee Processing By-Products: Sustainable Applications, 1st ed. Elsevier Publisher.
- Germán-Heins, J., Flury, M., 2000. Sorption of Brilliant Blue FCF in soils as affected by pH and ionic strength. Geoderma 97 (1), 87–101.
- Giles, C., Smith, D., 1974. General treatment and classification of the solute sorption isotherms. J. Colloid Interface Sci. 47, 755–765.
- Guo, Y., Zhao, J., Zhang, H., Yang, S., Qi, J., Wang, Z., Xu, H., 2005. Use of rice husk-based porous carbon for adsorption of Rhodamine B from aqueous solutions. Dyes Pigm. 66 (2), 123–128.
- Hale, S.E., Alling, V., Martinsen, V., Mulder, J., Breedveld, G.D., Cornelissen, G., 2013. The sorption and desorption of phosphate-P, ammonium-N and nitrate-N in cacao shell and corn cob biochars. Chemosphere 91 (11), 1612–1619.
- Hollister, C.C., Bisogni, J.J., Lehmann, J., 2013. Ammonium, nitrate, and phosphate sorption to and solute leaching from biochars prepared from corn stover (Zea mays L.) and oak wood (Quercus spp.). J. Environ. Qual. 42 (1), 137–144.
- Hou, J., Huang, L., Yang, Z., Zhao, Y., Deng, C., Chen, Y., Li, X., 2016. Adsorption of ammonium on biochar prepared from giant reed. Environ. Sci. Pollut. Res. 23 (19), 19107–19115.
- Jia, M., Wang, F., Bian, Y., Jin, X., Song, Y., Kengara, F.O., Xu, R., Jiang, X., 2013. Effects of pH and metal ions on oxytetracycline sorption to maize-straw-derived biochar. Bioresour. Technol. 136, 87–93.
- Kizito, S., Wu, S., Kipkemoi Kirui, W., Lei, M., Lu, Q., Bah, H., Dong, R., 2015. Evaluation of slow pyrolyzed wood and rice husks biochar for adsorption of ammonium nitrogen from piggery manure anaerobic digestate slurry. Sci. Total Environ. 505, 102–112.

- Langmuir, I., 1918. The adsorption of gases on plane surfaces of glass, mica and platinum. J. Am. Chem. Soc. 40 (9), 1361–1403.
- Lehmann, J., Gaunt, J., Rondon, M., 2006. Bio-char sequestration in terrestrial. Mitig. Adapt. Strat. Glob. Change 11, 403–427.
- Lehmann, J., 2009. Biochar for Environmental Management: Science and Technology. Earthscan, London, pp. 1–12.
- Li, J., Liang, N., Jin, X., Zhou, D., Li, H., Wu, M., Pan, B., 2017. The role of ash content on bisphenol A sorption to biochars derived from different agricultural wastes. Chemosphere 171. 66–73.
- Liu, J., Wan, L., Zhang, L., Zhou, Q., 2011. Effect of pH, ionic strength, and temperature on the phosphate adsorption onto lanthanum-doped activated carbon fiber. J. Colloid Interface Sci. 364 (2), 490–496.
- Liu, Z., Fei, B., Jiang, Z., Liu, X.E., 2014. Combustion characteristics of bamboo-biochars. Bioresour. Technol. 167, 94–99.
- Liu, Z., Zhang, F.-S., 2009. Removal of lead from water using biochars prepared from hydrothermal liquefaction of biomass. J. Hazard. Mater. 167 (1), 933–939.
- Mattson, J.S., Mark, H.B., 1971. Activated Carbon: Surface Chemistry and Adsorption from Solution. Marcel Dekker, New York.
- Mohan, D., Pittman, C.U., Bricka, M., Smith, F., Yancey, B., Mohammad, J., Steele, P.H., Alexandre-Franco, M.F., Gómez-Serrano, V., Gong, H., 2007. Sorption of arsenic, cadmium, and lead by chars produced from fast pyrolysis of wood and bark during bio-oil production. J. Colloid Interface Sci. 310 (1), 57–73.
- Mohan, D., Sarswat, A., Ok, Y.S., Pittman, C.U., 2014. Organic and inorganic contaminants removal from water with biochar, a renewable, low cost and sustainable adsorbent a critical review. Bioresour. Technol. 160, 191–202.
- Mukherjee, A., Zimmerman, A.R., Harris, W., 2011. Surface chemistry variations among a series of laboratory-produced biochars. Geoderma 163 (3), 247–255.
- Mullen, C.A., Boateng, A.A., Goldberg, N.M., Lima, I.M., Laird, D.A., Hicks, K.B., 2010.

 Bio-oil and bio-char production from corn cobs and stover by fast pyrolysis. Biomass Bioenergy 34 (1), 67–74.
- Murray, C.A., Parsons, S.A., 2004. Advanced oxidation processes: flowsheet options for bulk natural organic matter removal. Water Sci. Technol. Water Supply 4 (4), 113–119.
- Namasivayam, C., Kavitha, D., 2002. Removal of Congo Red from water by adsorption onto activated carbon prepared from coir pith, an agricultural solid waste. Dyes Pigm. 54 (1), 47–58.
- Netpradit, S., Thiravetyan, P., Towprayoon, S., 2004. Adsorption of three azo reactive dyes by metal hydroxide sludge: effect of temperature, pH, and electrolytes. J. Colloid Interface Sci. 270 (2), 255–261.
- Newcombe, G., Drikas, M., 1997. Adsorption of NOM onto activated carbon: electrostatic and non-electrostatic effects. Carbon 35 (9), 1239–1250.
- Reinhart, D.R., Basel Al-Yousfi, A., 1996. The impact of leachate recirculation on municipal solid waste landfill operating characteristics. Waste Manage. Res. 14 (4), 337–346.
- Ruthven, D.M., 1984. Principles of adsorption and adsorption processes. John Wiley and Sons, New York, US, pp. 464.
- Sepulveda, L.A., Santana, C.C., 2013. Effect of solution temperature, pH and ionic strength on dye adsorption onto Magellanic peat. Environ. Technol. 34 (8), 967–977.
- Sidey, V., 2016. On the effective ionic radii for ammonium. Acta Crystallogr. A 72, 626–633.
- Song, W., Guo, M., 2012. Quality variations of poultry litter biochar generated at different pyrolysis temperatures. J. Anal. Appl. Pyrol. 94, 138–145.
- Spokas, K.A., Novak, J.M., Venterea, R.T., 2012. Biochar's role as an alternative N-fertilizer: ammonia capture. Plant Soil 350 (1), 35–42.
- Yao, Y., Gao, B., Inyang, M., Zimmerman, A.R., Cao, X., Pullammanappallil, P., Yang, L., 2011a. Biochar derived from anaerobically digested sugar beet tailings: characterization and phosphate removal potential. Bioresour. Technol. 102 (10), 6273–6278.
- Yao, Y., Gao, B., Inyang, M., Zimmerman, A.R., Cao, X., Pullammanappallil, P., Yang, L., 2011b. Removal of phosphate from aqueous solution by biochar derived from anaerobically digested sugar beet tailings. J. Hazard. Mater. 190 (1), 501–507.
- Yao, Y., Gao, B., Zhang, M., Inyang, M., Zimmerman, A.R., 2012. Effect of biochar amendment on sorption and leaching of nitrate, ammonium, and phosphate in a sandy soil. Chemosphere 89 (11), 1467–1471.
- Yuan, J.-H., Xu, R.-K., Zhang, H., 2011. The forms of alkalis in the biochar produced from crop residues at different temperatures. Bioresour. Technol. 102 (3), 3488–3497.